Chapter 1

Study of Quasi-Dimensional Combustion Model of Hydrogen-Enriched Compressed Natural Gas (HCNG) Engines

Fanhua Ma and Roopesh Kumar Mehra

Additional information is available at the end of the chapter

http://dx.doi.org/10.5772/65753

Abstract

The reserves of the petroleum-based fuels are directly correlated with the increasing demand of human mankind for energy production. With the growing world populations, industries, vehicles, and equipment, energy demand leads to the search for the substitute of petroleum fuels, which can cater for the need of people today. Considering the current global economic crisis, the interest in alternative fuels is extremely high. It is known that there is a limited amount of fossil-based fuels as a sustainable energy source. The majority of the energy used today is obtained from the fossil fuels. Due to the continuing increase over the cost of fossil fuels, demands for clean energy have also been increasing. With this increasing demand for energy very soon the petroleum fuels will be depleted so researchers are focusing on to find the ways and means to generate cheap and abundant renewable and clean energy sources. Moving ahead with these plans, hydrogen-enriched compressed natural gas (HCNG) engines have emerged as a future energy carrier for an internal combustion engine. Several countries are striving hard to bring down the pollution level by promoting hydrogen-enriched compressed natural gas-fueled vehicles in general by powering heavy vehicles like transportation buses as well as passenger cars. In general, under certain conditions, the indicated thermal efficiency of the HCNG engine is much better than CNG engines without compromising the high level of pollutant emissions. Even so, the hydrogen addition to CNG increases the NO_x emission, due to high heat generated inside combustion chamber. This can be minimized by application of lean-burn combustion or with three-way catalyst.

Keywords: hydrogen enrichment, HCNG, lean-burn combustion, hydrogen generation, combustion

1. Introduction

Many activities had been performed not long ago on the operation of internal combustion engines on gaseous fuels including SI and CI systems. Such type of activities had induced the need to produce engines that can adhere with the latest demanding regulations for cleaner tail-pipe emissions. Natural gas is frequently thought of as the most auspicious alternative fuels for vehicles. Natural gas is a highly abundant fuel compared to petroleum and is usually regarded as the cleanest of the fossil fuels, producing significantly less harmful pollutant such as CO, CO_2, and nonmethane HC emissions than gasoline. On the other hand, by comparing natural gas to diesel, it roughly filters the very fine particles called as particulate matter. Natural gas contains high hydrogen carbon ratio and a high research octane number (RON) which prompts the exhaust to be cleansed and permits for high antiknocking properties. The availability of hydrogen as an element is ample on earth and is frequently considered as the standard optional fuel in future. However, the present available facility is not able to use hydrogen as a massive fuel efficiently. With regard to enhance the importance of hydrogen soon, hydrogen can be mixed with natural gas to be used in ICE engines. This new fuel is known as HCNG, or hythane, which can be used vigorously for transportation in the upcoming time.

Along with the experimental research of the HCNG engines, numerical simulations of the combustion process have been evaluated by many researchers in past three decade. This chapter mainly focuses on simulation of combustion mechanism of the HCNG and comparison with the experimental results, improvements on laminar burning velocity, and types of numerical model used for predicting the combustion behavior of the hydrogen-enriched compressed natural gas.

2. Background

The research on hydrogen-natural gas blends as IC engine fuel is not new. Natural gas-hydrogen mixtures have been used in test engines dating back to as early as 1983. The experiments performed with an AVL engine fueled by 100% CNG + 0% H_2, 80% CNG + 20% H_2, 50% CNG + 50% H_2, 0% CNG + 100% H_2 by Nagalingam et al. [1].

In the year 1989, at Colorado State University (Hythane Company, LLC, 2007), HCI (Hydrogen Components, Inc.) started testing different blending ratios of H_2 and natural gas. The patented blend of hydrogen and CNG was popularly given the name of 'Hythane' by Hydrogen Components, Inc., in Littleton, Colorado. With the reference of US Patient #5,139,002 (Lynch and Marmaro 1992), the invention of 'Hythane®' was done by Frank Lynch and Roger Marmaro, and in 1992, it was given a US patient. Here, hythane contains a blend of 15% hydrogen and 85% CNG, and it was used as a fuel for IC engines without any major modifications in the engine. The first hythane station was commenced in 1992. After that, many engines were manufactured and tested for using this new fuel, in order to understand the more significant

http://dx.doi.org/10.5772/65753

features of HCNG fuel. Still, the research is going on the areas related to spark timing, blend ratio, and excess air ratio.

3. Merits

Hydrogen addition to compressed natural gas (CNG) for use as a fuel in an internal combustion engine is an impressive way to improve the burning velocity, with a laminar burning velocity of 2.9 m/s for H_2 verses a laminar burning velocity of 0.38 m/s for CH_4, which is the constituent of the natural gas. It can increase the cycle-by-cycle variations (CCV) due to comparatively below par lean-burn capabilities of the natural gas engine. Hydrogen contains rapid combustion speed, a large combustion limit, and low ignition energy. All these unique properties of the hydrogen can lower the exhaust emissions of the fuel, especially the methane and CO emissions. The fuel economy and thermal efficiency of an engine can be improvised by hydrogen enrichment. The thermal efficiency of HCNG is covered in more detail in a research paper presented by Ma et al. [2].

Hydrogen-enriched compressed natural gas enables the use of hydrogen at an initial phase while utilizing support of the existing CNG system. Due to all these steps, the hydrogen infrastructure will be established, but meanwhile this process will take time till the generation and efficiency demands of the hydrogen can be met in an economical manner. The ideas and innovations involved in the research of the HCNG engines definitely are helpful for hydrogen engine research. The HCNG can allow to neglect bottlenecks coupled with evaporative emissions and cold-start enrichment, which is generally seen in gasoline engines.

4. Obstacles involved in HCNG as a fuel

Few new challenges are involved in the usage of the $H_2 + CH_4$ gas blend as a fuel. A major and vital challenge using HCNG as a fuel for internal combustion engines is to lessen the perfect H_2/CH_4 blend ratio. Whenever the percentage of hydrogen increases in the natural gas at a particular level, abnormal combustion such as pre-ignition, knocking, and back-fire, difficulty will take place until the ignition timing and A/F ratio are fully regulated. The reason behind this phenomenon is the exceptionally higher burning velocity of hydrogen and its low quench distance, which leads to the combustion cylinder walls to be hotter. The higher heat loss from the cooling water is also observed. As the hydrogen fraction increases into CNG, the lean operation limit shifted positive side, and the maximum brake torque (MBT) degrades, which leads to the meaningful fact that there exits relationship between hydrogen fraction, ignition timing, and excess air ratio. Hence, searching the optimum set of hydrogen fraction, ignition timing, and excess air ratio along with the other parameters that can be optimized is a typical challenge.

The addition of H_2 has the opposite effect on the hydrocarbon emissions, so it is necessary to compromise at a hydrogen ratio for which the NO_x and hydrocarbon emissions are equally

low. The emissions values of any fuels are probably the most important factor in determining whether or not the fuel is suitable as an alternative. However, the NO_x emissions for CNG are already extremely low compared to other traditional fuels like gasoline and diesel, but the addition of hydrogen causes increased NO_x emissions, which is not tolerable. Nowadays, emission control agencies of various countries are presenting more and more strict policies, so this is a challenge for all automobile manufacturing industries that they should more focus toward clean fuel like HCNG.

5. Hydrogen generation essential for HCNG adoption

Hydrogen production at low cost is the challenging task for present researchers. However, there are various advancements in existent technologies, and some new technologies are also on the platform for the production of hydrogen. Here, we sort out the hydrogen production methods into three subcategory, that is, hydrogen generation from fossil fuels, renewable sources of energy, and from biomass gasification. For future perspective, if existent CNG infrastructure will be replaced by HCNG ones, we need to generate more hydrogen at a reduced cost.

Technology	Merits	Demerits
Partial oxidation	Diminished desulfurization requirement, no catalyst requirement, high operating temperatures, low methane slip	Low H_2/CO ratio obtained Higher operation temperatures Complex handling process
Autothermal reforming	Lower process temperature than partial oxidation, low methane slip	Limited commercial experience Air/O_2 requirement
Steam reforming	Most developed industrial process, No O_2 requirement, lowest operating temperature, best H_2/CO ratio obtained	Highest air emissions

Table 1. A Comparison of fossil fuel reforming technology (modified from Ref. [3]).

The benefits and challenges to yield hydrogen and the methods are described in **Table 1**. At the end of the reforming process H_2, CO and CO_2 are protruded. For the smooth completion of the steam reforming process, it requires an external heat source but does not any demand of oxygen for the process. It has a less operating temperature and greater H_2/CO ratio than partial oxidation and autothermal reforming. Hydrocarbons are partially oxidized with O_2 to generate hydrogen. Partial oxidation (combustion) reaction is considered as the supreme source of energy to run this entire process. There is no catalyst required for this process, and it is more sulfur patient as compared to steam and autothermal reforming. The pressure requirement for the autothermal reforming is less than partial oxidation. There is no external energy required for partial oxidation and autothermal reforming. The complexity and expense of the system increase each of above processes, which require pure oxygen. As compared to

http://dx.doi.org/10.5772/65753

the other reforming process technologies for fossil fuels, steam reforming is less costly and most common method to generate oxygen [3].

The characteristic of coal by gasification was examined under the experimental condition limit, which is the temperature at 650–800°C, pressure at 23–27 MPa, and rate of flow 3–7 kg/h. As a catalyst, K_2CO_3 and Raney-Ni and H_2O_2 as oxidant were used. The important effects of key operation parameters like temperature, pressure, flow rate, oxidant, catalyst, and concentration of coal slurry upon gasification were investigated. They found from their experiments that the high temperature condition is favorable for the gasification of coal in supercritical water, but the pressure has no meaningful effect on the result of gasification, and flow rate influences some gasification results, in pursuance of the experimental condition optimal rate of flow should be selected. Also, they included that K_2CO_3 gives good catalytic effect as compared to Raney-Ni. The gasification efficiency and hydrogen gasification efficiency increase with the advancement of concentration of coal slurry, whereas carbon gasification efficiency decreases. Freni et al. [4] have carried out experiments and have described that the syn-gas production from natural gas, by both partial oxidation and autothermal processes, has been reviewed. The steam reforming reaction process produces hydrogen from methane (CH_4) that gives higher hydrogen to carbon monoxide ratio close to 3. Continuous heat supply is required for these reactions because of its strong endothermicity. Without using great amount of energy, partial oxidation and autothermal process are good option for producing hydrogen also if less ratio of H_2/CO (2–3) is achieved. Moreover, smaller reactors or high continuity is present and possible, because the partial oxidation is faster than catalytic methane reaction with steam (SRM). Steam reforming reactors sharply work at contact time ≈1 s, whereas partial oxidation can be lower than 10^{-2} [5].

There are various types of renewable energy sources, such as geothermal, solar, wind, from which we can produce hydrogen. Tolga Balta et al. [6] discussed hydrogen generation methods powered by geothermal sources. In this case study, a high temperature electrolysis (HTE) process compound with and based on geothermal source is considered. They found that HTE system consumes 3.34 kWh_e at 230°C and produces 573 mol/s H_2. The overall system is obtained to be 87 and 86% efficiencies of energetic and exergetic, respectively. Kanoglu et al. [7] developed four models for the use of geothermal energy source for hydrogen yielding; they used geothermal output as input for the electrolysis process (EP): in Case 1, part of heat from geothermal for producing work for EP; in Case 2, part of heat from geothermal in an EP to preheat H_2O; in Case 3, heat from geothermal to preheat water in a high temperature EP and using a portion of geothermal work for electrolysis; and the left portion for liquefaction in Case 4. The results explain that when the geothermal water temperature increases, the percentage of hydrogen generation increases. Moreover, 1.34 g of H_2 may be generated by 1 kg of geothermal water at 200°C in a reversible operation for Case 1, and 1.42, 1.91 and 1.22 are corresponding values for Cases 2, 3, and 4. They compared also in the reversible and irreversible situations display that the second-law efficiencies of models are 28.5, 29.9, 37.2, and 16.1% in Case 1, Case 2, Case 3, and Case 4, respectively.

The gasification means the conversion of the biomass into a highly inflammable gas mixture by the partial oxidation of biomass at very high temperatures rages of 800–900°C. The whole

process effectuates partial oxidation to transform carbonaceous feed stock gaseous energy conveyer take part of permanent, noncondensable gas mixture (CO, CO_2, CH_4, H_2, and H_2O). Basically in ideal gasification process, biomass transforms well enough to CO and hydrogen [8]. A most general known biomass resource is palm shell oil, and Cohce et al. [9] during his experimental investigations had studied the thermodynamic properties of the gasification process, which was followed by the SMR (steam methane reforming) and the various reactions involved in the process. During his experimental investigation made by a simulation tool, observations revealed regarding H_2 production using thermochemical biomass gasification using energy and exergy methods. Focus was also laid on evaluating the efficiency of H_2 generation from biomass. The moderateness of the H_2 generation from biomass and a crucial ability of biomass as a renewable energy source have been get through by considering two methods: (1) the heat expected for steam CH_4 reforming is supplied by fractioned syn-gas and (2) the steam methane reformer combustion reactor with externally supplied CH_4 gas. For the direct gasification process, a BCL-type low temperature indirectly heated steam gasifier is investigated. The simulation results show that on the basis of performance improvements, second case has higher energy and exergy efficiencies than first case.

The largest sources of organic waste are our houses, for example, food waste, lawn clippings, and also add the animal- and plant-based material and degradable carbon such as paper timber. Nielsen et al. [10] demonstrated pure hydrogen extraction from fermentation of waste from houses using anaerobic bacterial flora in a mixed form. The experiment was simulated in a bioreactor where 600 g waste from house was fermented. The bioreactor was continuously sprayed with gas N_2 at 3 ml/min and enters in from lower part. They found that throughout this study about 85–90% of the H_2 was separated by Pd/Ag membrane and also observed that ZnO did not expunction meaningful quantity of H_2.

Wu et al. [11] have done their experiments on waste wood gasification and were performed with scale gasification. They investigated the main factors on which hydrogen production depends in the noncatalytic process and catalytic process. The temperature influences the process involved; thus, it is indicated as most important factor of this experimental study and authors concluded that pure H_2 can be obtain from biomass of wood waste through high temperature gasification and reforming techniques. The synthesis gas (54% hydrogen yield by volume) obtains from feedstock at 950°C without a catalyst was reported. Use of catalyst like commercial steam reforming Ni catalyst improves the hydrogen yield at 750°C.

6. Fundamental properties of HCNG

There is a one impressive and very effective way to mix CNG with the fuel holds fast burning velocity. The high flame burning velocity and wide range of flammability limits in air make hydrogen the best gaseous option for CNG. The combination is anticipated to raise the lean-burn capability characteristic and lower the harmful engine's tail pipe emissions [12, 13]. **Table 2** lists few properties of hydrogen compared to CNG (methane) and gasoline. It is clearly observed that hydrogen and CNG have a similar combustion property. Hydrogen utilization

in spark ignition engines as a charge gives significant improvements in the overall performance. The mixture of hydrogen and air has higher self-ignition temperature as compared to the different fuels; therefore, the presence of hydrogen creates an antiknock quality of fuel along with higher ignition temperature and lower flame luminosity, which makes it as a safe and clean fuel in comparison with the other conventional fuels [14]. A fusion of the little amount of hydrogen with air induced a flammable mixture, which can be fired in a combustion chamber of a conventional SI engine at below the lean combustion limit of gasoline/air mixture. The combustion of this highly lean mixture lowers the flame temperature and results directly to less heat transfer to the cylinder walls, higher the engine thermal efficiency, lower is the oxides of nitrogen exhaust emissions.

Fuel	**CNG**	**H_2**
Molecular weight	16.04	2.02
Equivalence ratio ignition lower limit in NTP air	0.1	0.53
Flammability limits	5~15	4~75
Minimum ignition energy (mJ)	0.29	0.02
Ignition temperature	918	858
Mass lower heating value (kJ/Kg)	119,930	50,000
Density of gas NTP (kg/m^3)	0.083764	0.65119
Quenching gap in NTP air (cm/s)	0.203	0.064
Percentage of thermal energy radiated	23–33	17–25
Diffusivity in air (cm^2/s)	0.2	0.63
Quality LHV	50.03	120
Volume LHV	35.37	10.805
Octane number	107.5	>130
Adiabatic index	1.315	1.142
Volumetric lower heating value at NTP (kJ/m^3)	10,046	32,573
Stoichiometric air-to-fuel ratio	34.20	17.19
Volumetric fraction of fuel in air, $\lambda = 1$	0.290	0.095
Volumetric lower heating value at NTP (KJ/m^3)	10,046	32,573
Stoichiometric air-to-fuel ratio	34.20	17.19
Volumetric fraction of fuel in air, $\lambda = 1$	0.290	0.095
Volumetric lower heating value in air, $\lambda = 1$	2913	3088
Burning speed in NTP air (cm/s)	265–325	37–45

Note: NTP denotes normal temperature (293.15 K) and pressure (1 atm).

Table 2. Properties of H_2 compared with methane (CH_4).

The laminar burning velocity of the hydrogen/air mixture is about six times as compared to the gasoline/air. This high laminar burning velocity of the hydrogen resulted that the actual indicator diagram shifted toward near to the ideal indicator diagram and produces the higher thermal efficiency of the engine [15]. Hydrogen has possessed wide variety of flammability limits with flammable mixtures from highly lean $\lambda = 10$ to highly rich $\lambda = 0.14$ ($\varphi = 0.1$–7.1). This provides a wide range of engine power output via changes in the blends excess air ratio. The flammability limits get more widen with improving temperature [16]. The minimum ignition energy of the H_2 + air blends at NTP condition is much lower than that of CH_4 + air and gasoline + air mixtures. Only 0.017 mJ, minimum energy, is required for the combustion of 20–26% hydrogen air mixture. As minimum ignition energy is generally calculated using an electric spark discharge, and it also depends on the gap between two electrodes. The spark gap for the above-quoted data is 0.5 mm. Using a spark electrode gap of 2 mm, the minimum ignition energy required is 0.05 mJ [17]. Methane gas (CH_4) is major part of the compressed natural gas (CNG) having less carbon atoms; therefore, the combustion of CNG is considered to be favorable clean fuel as gasoline and also produces less environmental effect. However, because of its lean-burn capacity and lazy burning velocity, CNG-powered spark ignition engines still have few demerits such as low thermal efficiency, low power output, large cycle by cycle variation, and these all increase specific fuel consumption [18].

Although hydrogen is an alternative fuel with very clean burning characteristics, in spite of having disadvantages like high flame propagation speed and wide flammability range. The weight of hydrogen storage, its complexity, the loss of power associated through the usage of pure hydrogen, and the backfire phenomenon are some of the factors to be thought over. The backfire problem can be solved by adding high percentage of hydrogen to CNG. Hythane is basically a blend of 15% hydrogen and 85% CNG and was patented by Frank Lynch of Hydrogen Components Inc., USA, by its energy content [19]. In many cases, backfire restricts the operating region of the air-fuel mixture on the 'rich' side. With the natural gas addition, stoichiometric mixtures can be run without any other precautions.

Coppens et al. [20] with an all-inclusive error of the laminar burning velocity was obtained to be less than ±0.8% cm/s when hydrogen fraction in the mixture was increased from 0 to 35%. The constant volume bomb with spherically expanding flames has very popular in an estimation of a laminar burning velocity along with the growing flame visualization technology in recent years, due to its enhanced accuracy and its ability of estimating few other flame-associated variables together with Markstein constant [21]. In the past years, laminar burning velocity of HCNG fuel was evaluated by many researchers at different hydrogen fractions (volume fraction $R_H = 0$–100%) and equivalence ratio ($\varphi = 0.6$–1.4) [20, 22–24]. On the basis of experimental data, Huang et al. [22] proposed an empirical relation, which utilizes the conception of velocity increment. Equation (1) represents the formula of laminar burning velocity at NTP for CH_4 + air mixture

$$S_{l\_CH_4}(\phi) = -150.84\phi^3 + 287.6\phi^2 - 96.327\phi - 1.2924. \quad (1)$$

For hydrogen + air mixture, the following formula is used for calculating laminar burning velocity at NTP

$$S_{l\_H_2}(\phi) = 51.902\phi^3 - 394.46\phi^2 + 835.14\phi - 267.07. \tag{2}$$

And Eq. (3) is defined as the laminar burning velocity increment

$$\frac{\left[S_{L\_HCNG}(\phi) - S_{L\_CH_4}(\phi)\right]}{\left[S_{L\_H_2}(\phi) - S_{L\_CH_4}(\phi)\right]}, \tag{3}$$

where $S_{L\_H_2}(\phi)$ and $S_{L\_CH_4}(\phi)$ are laminar burning velocity of hydrogen and natural gas (methane). Laminar burning velocity of hydrogen and methane can be determined by the following empirical relation:

$$S_L = A(T^0)Y_{F,u}^m \frac{T_u}{T^0}\left(\frac{T_b - T^0}{T_b - T_u}\right)^n \tag{4}$$

$$T^0 = -E / \mathrm{In}\left(-\frac{p}{B}\right) \tag{5}$$

$$A(T^0) = F\exp\left(-\frac{G}{T^0}\right), \tag{6}$$

where $Y_{F,u}$ is a fuel fraction in unburned charge, p is the pressure, and T_u and T_b are temperature of unburned and burned zone. Other unknowns like constants *B, E, F, G, m,* and *n* can be calculated by properties of fuel used [25]. The increments of the laminar burning velocity on the basis of hydrogen fraction are shown in **Figure 1**. With the rise of hydrogen fraction, the increment of laminar burning velocity increases exponentially. It is observed by Ma et al. [26], and they proposed the correlation between these two parameters for HCNG (Eq. 7)

$$\frac{\left[S_{L\_HCNG}(\phi) - S_{L\_CH_4}(\phi)\right]}{\left[S_{L\_H_2}(\phi) - S_{L\_CH_4}(\phi)\right]} = 0.00737\exp\left(\frac{x}{20.38}\right) + 0.00334. \tag{7}$$

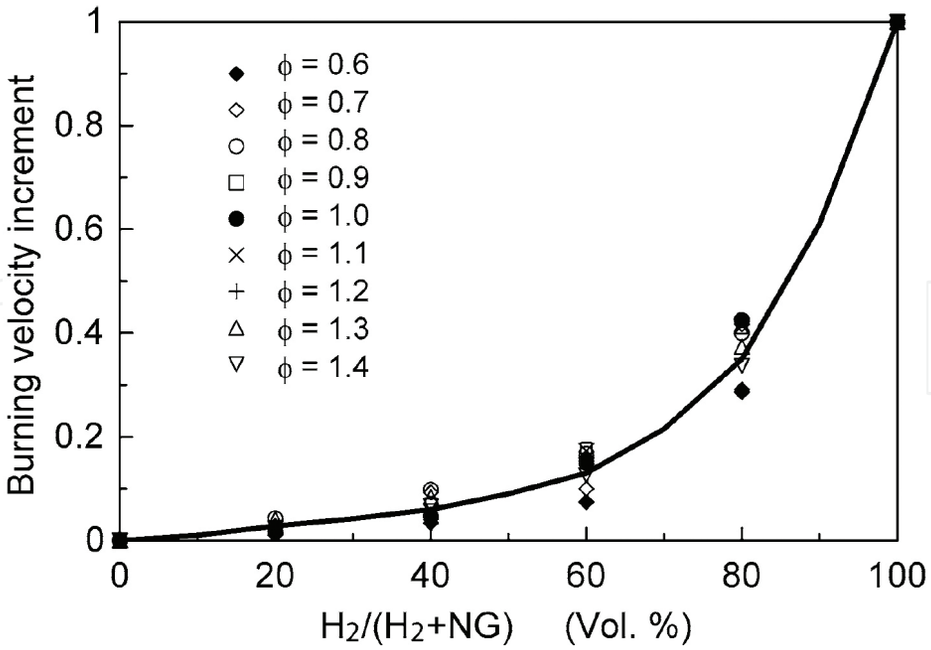

Figure 1. Burning velocity increment versus hydrogen fraction at different equivalence ratios [22].

Hence, the laminar burning velocity at various hydrogen volume percentage and equivalence ratios can be determined by using formula (2), and (7). After proposing Eq. (7), they checked its accuracy. The values determined by formula (Eq. 7) are compared with the experimental data, which are displayed in **Figure 2**, and the comparison is depicted in **Table 3**.

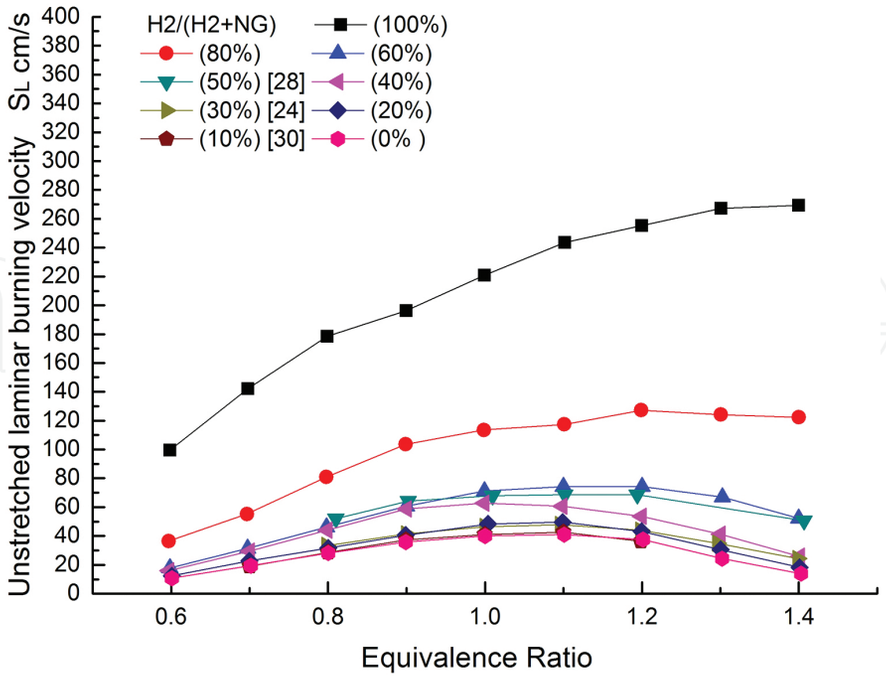

Figure 2. Laminar burning velocity of HCNG versus equivalence ratio [20, 22–24].

Φ	R_H						
	10	**20**	**30**	**40**	**50**	**60**	**80**
0.6		−2.6		2.6		−27.6	−13.7
0.7	11.6	2.6		12.2		−14.6	−12
0.8	−6.2	0.5	0.1	17.6	21.5	−5.1	0.8
0.9	−2.2	3.1	0.4	24.5	23.1	5.4	11.8
1	−4.2	8.5	0.4	20.7	18.4	9.4	9.5
1.1	−3	8.4	−0.1	14.5	15.4	8.1	5.4
1.2	−12.7	1.5	−2.5	8.15	18.4	9.8	11.2
1.3		2.3	6.5	9.2		14.8	12.7
1.4		−7.8	6.8	−6.6	29.8	7.5	16.3

Table 3. Comparison of the experimental value in **Figure 4** with calculated ones from Eq. (7).

From the **Table 3**, it is clearly observed that the experimental data of laminar burning velocity of HCNG are quite close to the determined values at low and high hydrogen fractions (0% < R_H < 60% and 60% < R_H < 100%). Nevertheless, for medium hydrogen fraction (30% < R_H < 60%) condition, it is found that the errors are quite high (>15%). According to procure, a correlation of the laminar burning velocity of HCNG is reasonable at medium and large hydrogen fractions and at various φ. The authors further examined the feasibility of a Le Chatelier's rule-like formula, which is depicted as follows:

$$S_{L\_HCNG}(\phi, x) = \frac{1}{x / S_{L\_H_2}(\phi) + (1-x) / S_{L\_CH_4}(\phi)}. \tag{8}$$

Φ	R_H					
	10	**20**	**30**	**40**	**50**	**80**
0.6		−5.3		−5		−2.9
0.7	−11.4	−3		−0.2		−13.5
0.8	−7.2	−6.8	−12.9	3.5	6.6	−6.7
0.9	−4.2	−5.2	−14.3	9.5	5.7	0.2
1	−6.2	0.8	−14.2	5	0.04	−2.3
1.1	−4.5	1.1	−14	−1.2	−2	−4.2
1.2	−13.2	−5.1	−14.9	−6.4	4.5	7
1.3		2.5	4.3	7.1		28.2
1.4		6	20.2	13.5	47.7	52.9

Table 4. Comparison of the experimental value in **Figure 4** with calculated ones from Eq. (8).

With the similar procedure, they compared the experimental and determined data through Le Chatelier's rule-like formula, and the results are tabulated in **Table 4**. It is observed that the values determined from Formula (8) are agreed with the experimental laminar burning velocity of HCNG at lean and stoichiometric conditions.

Miao et al. [27] studied flame propagation of assorted CNG/H_2/air mixtures in fixed volume combustion chamber under miscellaneous hydrogen volume percentage and equivalence ratios along with miscellaneous initial pressures. The flame stability and their impressing factors like Markstein length, density ratio, and flame thickness were acquired by analyzing flame image at various hydrogen volume percentage, initial pressure, and equivalence ratios. This experimental study concluded that at initial pressure, hydrogen volume percentage and equivalence ratio attempt a combined influence on unstretched laminar burning velocity and mass burning flux of CNG/H_2/air mixtures, and both abruptly increase along with the hydrogen enrichment in the natural gas.

7. Technical approach

Performance plays an important role in the choice of a fuel. HCNG has many advantages when it comes to performance because of the high octane number of hydrogen, and the engine performance generally increases with the addition of hydrogen. Generally, excess air ratio (λ), ignition timing, engine speed, and compression ration influence the performance of the engine greatly.

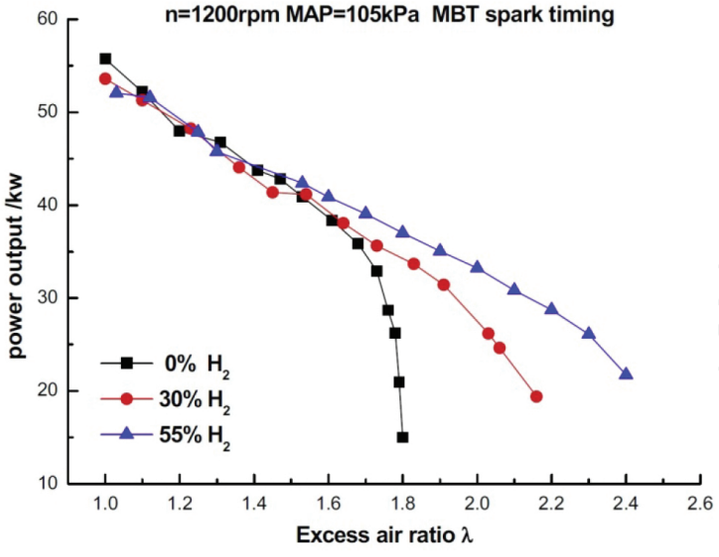

Figure 3. Engine's power performance versus excess air ratio [28].

Ma et al. [28] observed the influence of high volumetric ratio of hydrogen to CNG (55% H_2 + 45% CNG). The performance and emission characteristics were analyzed in a six-cylinder, single-point injection, turbocharged lean-burn natural gas engine. The experimental results

http://dx.doi.org/10.5772/65753

revealed that using H_2 at a high volumetric ratio significantly increases in the lean-burn combustion limit and improves thermal efficiency. **Figure 3** shows that high H_2 enrichment to CNG gives high impression to slow down the decline in power. As excess air ratio increases, power output decreases, this is because of injected fuel quality degraded with the increasing λ, and outcome is the reduction in input energy of the engine, in addition. When $\lambda > 1.6$, HCNG gives more power output as CNG. It is shown in **Figure 4** that the mixing of H_2 at a high ratio in CNG significantly improves the lean-burn limit along with the higher thermal efficiency. The same effects have seen in another experimental study of the same the author [29].

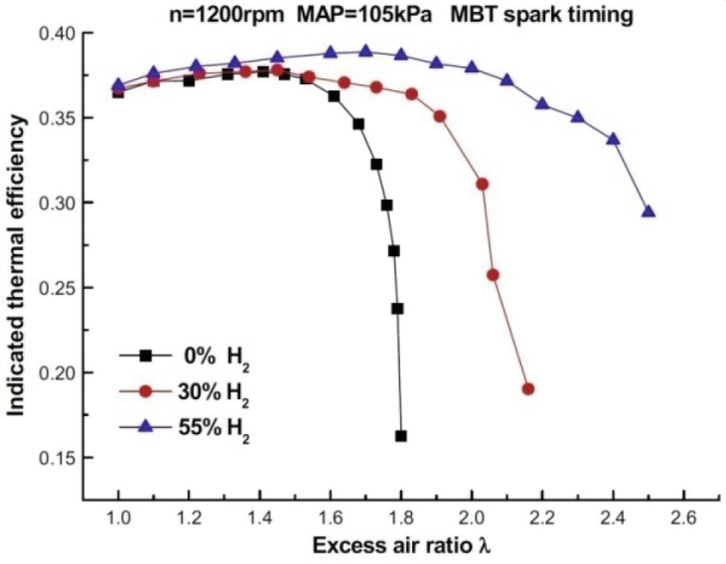

Figure 4. Indicated thermal efficiency versus excess air ratio [28].

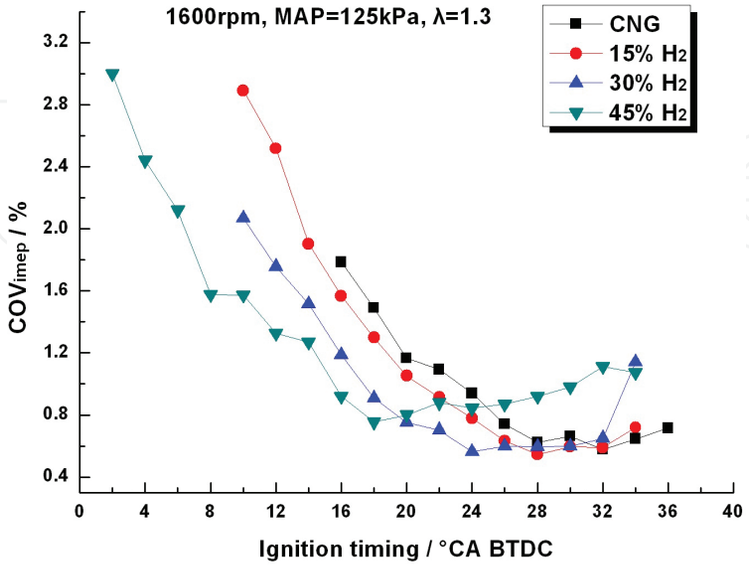

Figure 5. COV in IMEP versus ignition timing for fuel blends with various hydrogen fractions [30].

With respect to study the mechanism of the combustion of any fuel, the cycle-by-cycle variation (CCV) study of engine is very beneficial. It gives the clear picture of maximum pressure and mean effective pressure developed, which affects the power and efficiency of the engine. As discussed already that the COV_{imep} is an important factor to analyze combustion. Ma et al. [30] did experiments for investigating the consequences of addition of hydrogen on the combustion characteristic and CCV in a 6.2-liter, in-line six-cylinder turbocharged SING engine. The ITE and emissions were also analyzed through the series of experiments. They concluded that advancing the spark timing gives improved maximum pressure for used fuel blends. **Figure 5** shows the variation of the COV_{imep} versus ignition timing at different hydrogen fractions. With the increase in the spark advance, the COV_{imep} decreases significantly. Addition of H_2 into NG can lower the COV_{imep} at every spark timing, retarded from maximum brake torque spark timings.

Burning of fuel at lean condition ($\lambda > 1$) provides lower combustion temperature, and it is proved by many researchers that this is a meaningful and beneficial way to reduce NO_x emission, in the case of spark ignition engines only [31, 32]. Various authors have performed their research by adopting constant spark timing condition. But it is not enough information to predict the influence of ignition timing on combustion. Wang et al. [33] studied separately the influence of ignition timing on lean combustion limit through their series of experiments on the HCNG SI engine. The low and moderate engine load, various engine speeds and 0–40% by volume hydrogen fraction condition are adopted for experiments. **Figure 6** illustrates the consequence of ignition timing on lean combustion limit using three different conditions. The lean combustion limit improves with the advance of spark timing, and after reaching maximum value, it shows decreasing trend. This is because of the enough amount of fuel burned in the power stroke instead of near the completion of compression stroke. Moreover, they stated that over-retarded and over-advanced both ignition timings are not appropriate for smooth combustion at lean combustion limit at a particular operating condition.

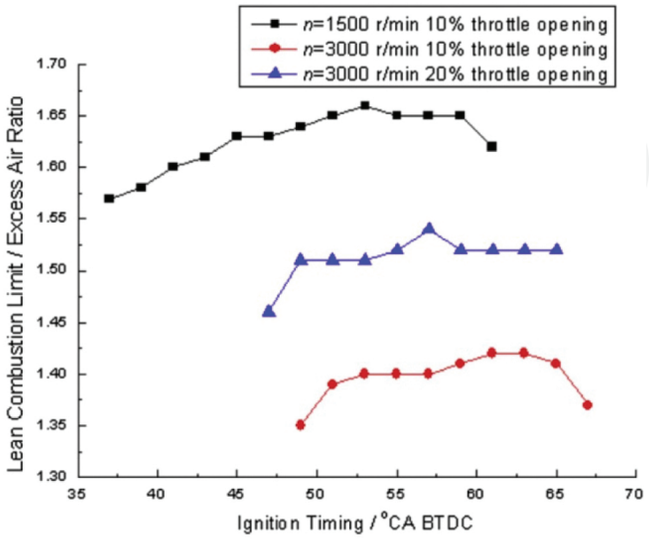

Figure 6. Effect of ignition timing on lean combustion limit [33].

http://dx.doi.org/10.5772/65753

An engines' behavior under idle conditions regarding fuel consumption and emissions is very important. A large part of driving cycle used in regulations like the New European Driving Cycle (NEDC) takes place at idle speed. Furthermore, real driving situations, especially in traffic jam haunted Asian megacities, may contain even more idling percentage. Ma et al. [34] experimentally investigated the effect of the equivalence ratio (φ) and spark advance angle (θ_i) on the idle behavior (engine speed 800 rpm) of the six-cylinder, single-point injection turbocharged hydrogen-fueled SING engine. They stated that with the increase in φ, the value of spark advance angle (θ_i) corresponding to the maximum ITE gradually decreases, whereas the ITE decreases along with an increasing φ. Under the condition of $\varphi \geq 0.6$, The NO_x emission increases with an increasing φ and θ_i. At lower φ and θ_i, COV_{imep} noticeably increases. The maximum cylinder pressure increases along with an increasing φ and θ_i. They reported that the optimum idle conditions (considering COV_{imep}, fuel consumption, emission performance) are $\varphi = 0.4$ and $\theta_i = 18°CA$. These conditions provide the 20% rise in ITE and 5 ppm lowered NO_x emission.

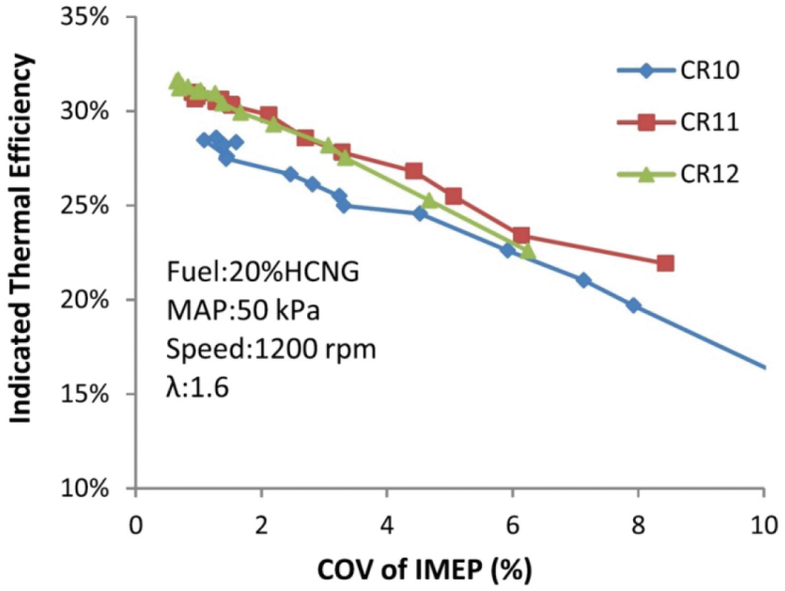

Figure 7. Variation in indicated thermal efficiency with COV of IMEP [35].

Many researchers studied the effects of compression ratio (CR) on the performance and emission characteristic of the hydrogen-enriched CNG engines. Ma et al. [35] investigated the effect of compression ratio (CR) and ignition timing on an in-line, six-cylinder, single-point injection, turbocharged SING engine. The experiments were performed under the condition of varying the ignition time with three different compression ratios of 10, 11, and 12. The engine speed was kept constant at 1200 rpm; excess air ratio was fixed at 1.6, and a constant manifold absolute pressure (MAP) of 50 kPa was selected for the tests. Based on their experimental data, they mentioned that with increasing compression ratio, it could be possible to achieve higher indicated thermal efficiency. The observations of the experimental study show that leading compression ratio gives improved brake torque and less brake-specific fuel consumption and

increased peak pressure. It is found that at higher compression ratio, the heat release rate gets faster. As the indicated thermal efficiency increases, the COV of IMEP decreases and increasing CR can lower COV of IMEP as illustrated in **Figure 7**. Also, the rapid combustion period and early flame developments are reduced.

8. Quasi-dimensional combustion models

A quasi-dimensional model (QDM) is very popular to analyze the combustion process of the engine. Quasi-dimensional models have executed more precise results and also have the ability to describe a combustion process more accurately, due to two-zone consideration (unburned and burned) [36]. Ma et al. [26] presented a two-zone quasi-dimensional combustion model for HCNG SI engines with various hydrogen volumetric fractions. A two-zone (burned and unburned) thermodynamic model, turbulent entertainment combustion model, and important thermochemical equation were introduced. Simulation data were examined and compared by experimental data after getting the model constant by calibration for different hydrogen percentage, ignition timings, and equivalence ratios. It is observed that simulation results are quite near to the experimental results for lean conditions. **Figure 8** shows the two-zone combustion chamber for which the two-zone thermodynamic model was presented by assuming some assumptions. The following control equations are derived by the authors of this research paper based on mass and energy conservation law for two-zone thermodynamic models.

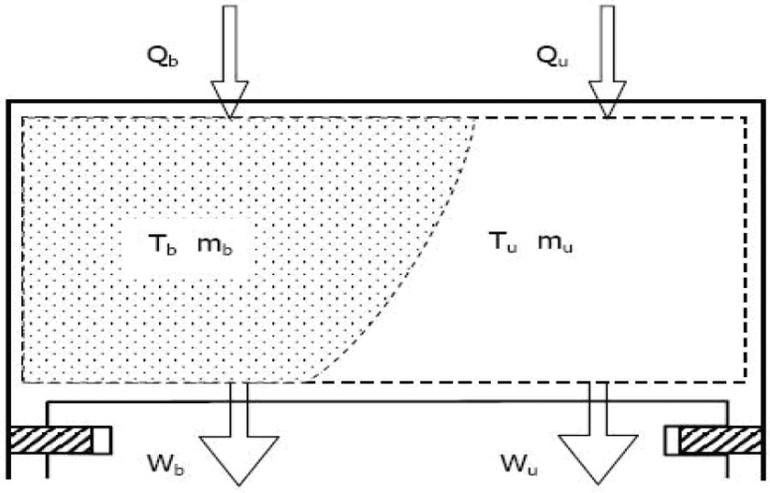

Figure 8. Two-zone combustion chamber [26].

$$\frac{dT_u}{d\theta} = \frac{1}{m_u c_{pu}}\left(V_u \frac{dP}{d\theta} + \frac{dQ_u}{d\theta}\right) \tag{9}$$

$$\frac{dT_b}{d\theta} = \frac{1}{m_u c_{pu}}\left[P\frac{dV}{d\theta} - \left(R_b T_b - R_u T_u\right)\frac{dm_b}{d\theta} - \frac{R_u}{c_{pu}}\left(V_u \frac{dP}{d\theta} + \frac{dQ_u}{d\theta}\right) + V\frac{dP}{d\theta}\right] \tag{10}$$

$$\frac{dP}{d\theta} = \frac{1}{\frac{c_{vu}}{c_{pu}}V_u - \frac{c_{vb}R_u}{R_b c_{pu}}V_u + \frac{c_{vb}}{R_b}V}\left\{\left(1+\frac{c_{vb}}{R_b}\right)P\frac{dV}{d\theta} - \frac{dQ}{d\theta} + \left[\left(u_b - u_u\right) - c_{vb}\left(T_b - \frac{R_u}{R_b}T_u\right)\right]\frac{dm_b}{d\theta} + \left(\frac{c_{vu}}{c_{pu}} - \frac{c_{vb}}{R_b}\frac{R_u}{c_{pu}}\right)\frac{dQ_u}{d\theta}\right\}, \tag{11}$$

where u and b represent unburned zone and burned, respectively. The charge composition of the each zone is considered to be ideal gas means specific heats are only the function of temperature. The specific heat (molar) at constant pressure is expressed by the equation below

$$C_{p,m} = a_1 + \frac{a_2}{\theta} + \frac{a_3}{\theta^2} + \frac{a_4}{\theta^3} + \frac{a_5}{\theta^4}\left(1200K < T < 6000K\right) \tag{12}$$

$$C_{p,m} = a_6 + a_7\theta + a_6\theta^2 + a_6\theta^3 + a_6\theta^4 (200K < T < 1200\,K), \tag{13}$$

where θ represented by T/1000 and constants a_1–a_{10} can be determined by Ref. [37]. The specific heat (molar) of the various blend is determined by the following expression.

$$C_{p,m} = \sum C_{p,m,i} X_i, \tag{14}$$

where X_i represents molar fraction of species i. After comparing the simulation and experimental data, authors concluded that the presented two-zone quasi-dimensional model has the capability to conduct a performance simulation of a HCNG SI engine under different hydrogen enrichment ratios.

The fluid flow in the combustion chamber is largely turbulent. The turbulent structure of flame front regulates the combustion process notably. In compliance with the assumptions presented by Blizard, Keck, and various other researchers [38–40], large-scale turbulence is suppose to comprise highly dissipative regions of vortex sheets and the size corresponding to the Kolmogorov scale (η). Their spacing is proposed by the Taylor microscale (L_T) as shown in

Figure 9. L denotes the integral length scale and corresponds to the overall size of the turbulent eddy. Later, this structure was justified by Smith [41]. Daneshyar and Hill [42] conceived that for the spark ignition engine, Taylor microscale (L_T) is very important for the better understanding of the combustion behavior. Their study reveals that chemical reaction completed almost quickly with in the Kolmogorov scale.

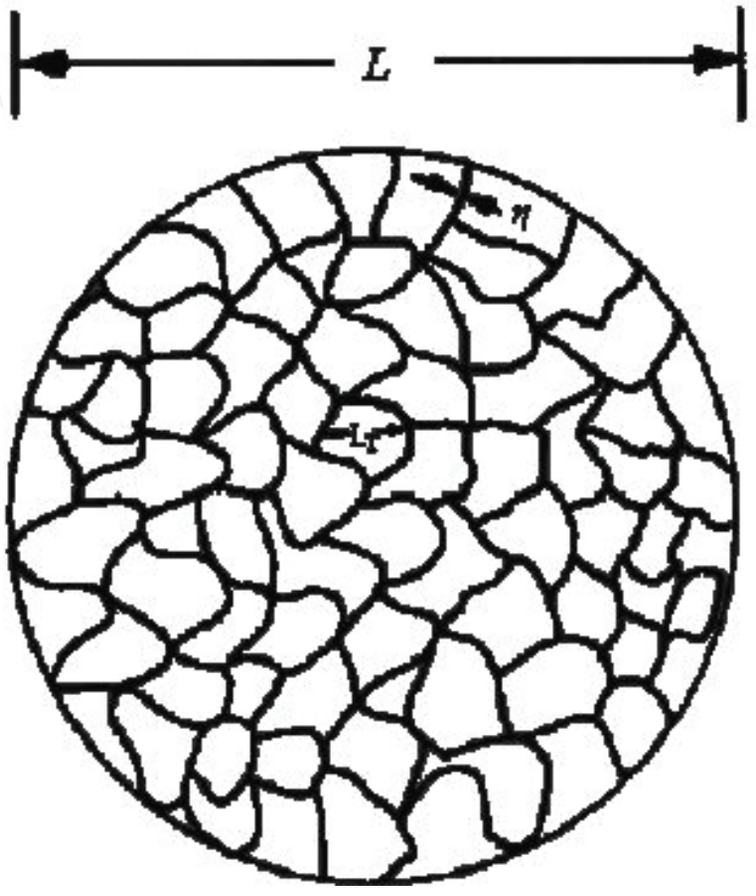

Figure 9. Schematic of the turbulence structure.

The model is presented by the authors of Ref. [26] and following this idea, it presumes as per Refs. [43, 44] that:

1. Ignition happens within the highly dissipative areas (vortex sheets) whose size is described by the Kolmogorov scale.
2. After spark, the ignition sites propagate along the vortex sheets with a velocity of $u' + S_L$ spherically, where u' is denoted by local turbulence intensity.
3. The flame front propagation is considered to be laminar process inside the spacing of the vortex sheets. Therefore, the combustion time span for a small eddy with the size of L_T is $\tau_c = L_T/S_L$.

The following governing equations could be derived by considering the above assumptions:

The rate of the entrainment of the unburned gas is as follows:

$$\frac{dm_e}{dt} = \rho_u A_f \left(S_L + u'\right) \tag{15}$$

In the above equation, m_e is denoted by mass entrained into the flame front; ϱ_u is the density of the gas in the unburned zone; and A_f is the area of the entrainment front.

Once entrained, the unburned gas will be burnt at a rate proportional to the mass of the unburned gas within the entrainment front, which is given by the following:

$$\frac{dm_b}{dt} = (m_e - m_b)/\tau_c \tag{16}$$

$$\tau_c = L_T / S_L, \tag{17}$$

where m_b is the mass burned, τ_c is the characteristic time, and L_T is the Taylor microscale.

By combining Eqs. (15) and (16), we can get the following:

$$\tau_c \frac{d^2 m_b}{dt^2} + \frac{dm_b}{dt} - \frac{dm_e}{dt} = 0. \tag{18}$$

Equation (18) provides a burning law model that can be coupled to the thermodynamic, turbulent eddy structure, and the turbulent characteristics, which are correlated to the hydrogen blending ratios and the engine operating conditions. The method of calculating the three turbulence scales is briefly described here:

Integral length scale L:

$$L_0 = C_L \times H \tag{19}$$

$$L = L_0(\rho_{u0} / \rho_u)^{1/3}, \tag{20}$$

where ϱ_u is the density of the gas in the unburned zone, H is the chamber height, and the subscript 0 represents ignition timing. Taylor microscale L_T

$$L_T = 0.8 L_{iv}(\rho_{in} / \rho_{u0})^{3/4}, \tag{21}$$

where ϱ_{in} is the density of gas in the intake stroke, and L_{iv} is the lift of the intake valve.

Turbulence intensity u′ is as follows:

$$u_0' = C_u \times C_m \tag{22}$$

$$u' = u'_0(\rho_{u0} / \rho_u)^{1/3}, \tag{23}$$

where C_m is the mean velocity of piston movement, C_u is a constant, and 0 represents ignition timing. To justify the suggested quasi-dimensional combustion model, experiments below a broad range of functioning state are required. **Table 5** displays the nine operation conditions which are chosen for both experiments and simulation. The limit of nine operating conditions is slightly broad, in which speed (N), manifold absolute pressure (MAP), hydrogen mixture ratio (x), excess air ratio (λ), and spark timing (θ_{ig}) all are modified extensively.

Operational condition	Speed N (r/min)	MAP (kPa)	x (%)	λ	θ_{ig} (BTDC)
X1	1600	70	20	1.3	26
X2	1600	120	20	1.3	26
X3	1600	87	40	1.20	24
X4	1600	65	50	1.25	22
Y1	1200	105	10	1.33	30
Y2	1200	105	30	1.40	30
Y3	1200	105	0	1.63	30
Y4	1200	105	30	1.62	30
Z1	2400	80	0	1.30	32

Table 5. Operating conditions.

The experiments were evaluated on a six-cylinder, single-point injection, spark ignition gas engine. **Figure 10** illustrates the predicted and experimental pressure curves and mass fraction curves at each operating condition. For operating condition H, the predicted and experiment values are quite matched. The divergence in Case H is thought to be due to high cyclic variation and incomplete combustion, which are not considered in the quasi-dimensional model. With regard to make significant observations, more detailed combustion parameters are analyzed, including maximum pressure (P_{max}), the crank angle at which maximum pressure occurs (θp_{max}), rapid combustion duration (θ_{rd}) (10–90% MFB), crank angle of 50% MFB ($\theta_{50\%}$), indicated mean effective pressure (P_i), and P_i's relative error (εp_i), again considering Case H and the differences between the predicted and test outcomes are pretty close. **Table 6** displays the differences between the predicted and experimental results. It can be seen that the P_{maxs} shows error <0.15 MPa; (θp_{max})'s, θ_{rd}'s, and $\theta_{50\%}$'s value is <2°CA; P_i's <6%. The most evident difference appears at Case H, and the equivalence ratio is close to the lean limit.

http://dx.doi.org/10.5772/65753

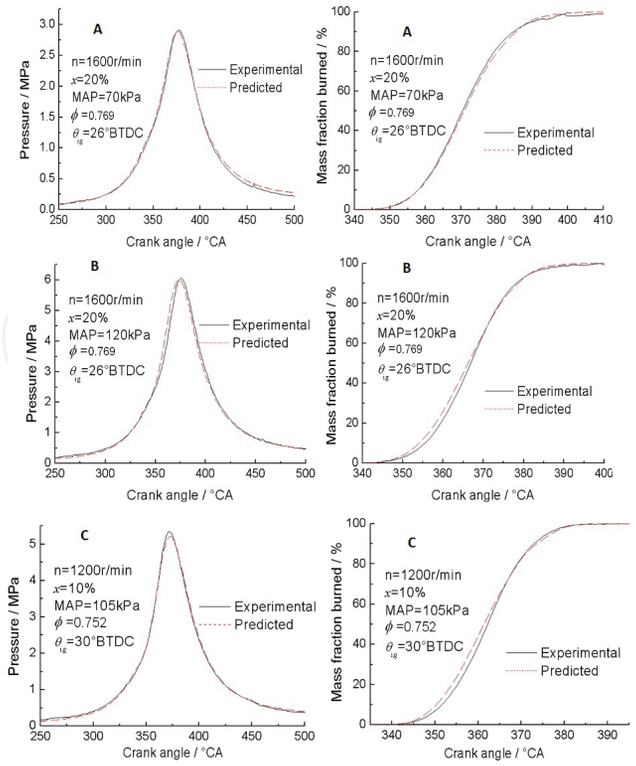

Figure 10. Comparison between experimental pressure, MFB, and predicted ones from the model under nine operating conditions.

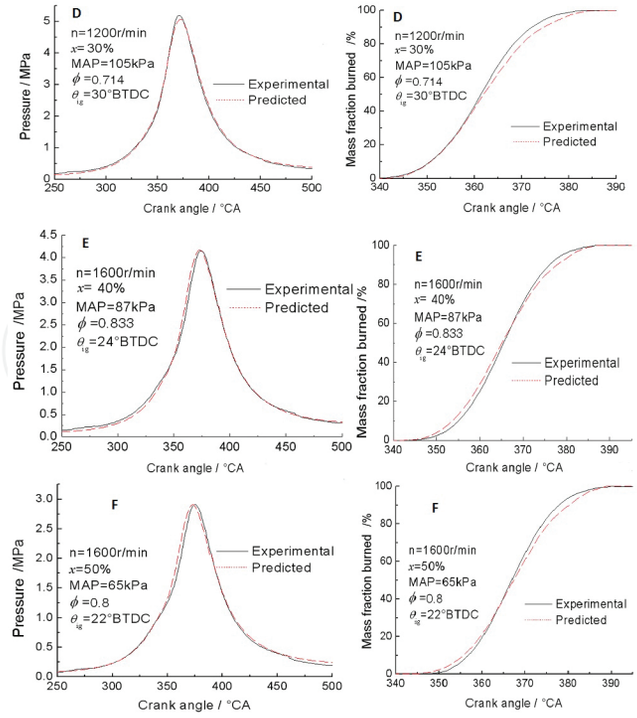

Figure 10. (continued)

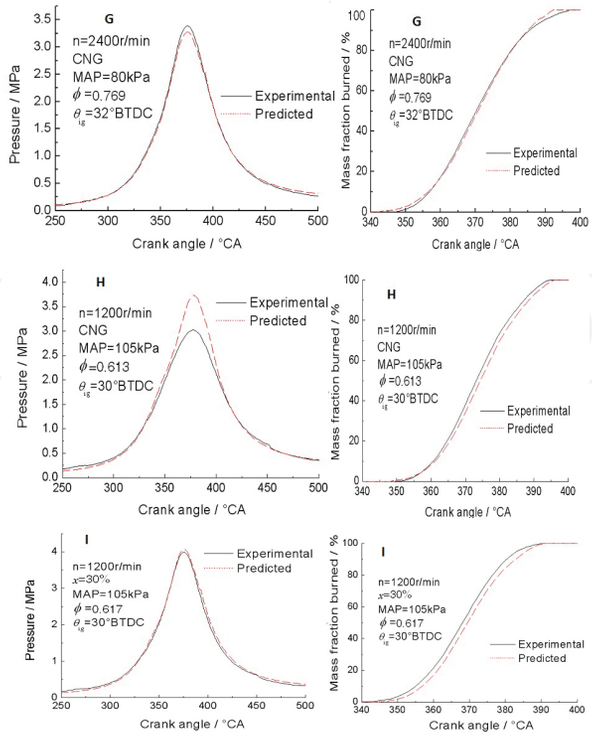

Figure 10. (continued)

Operation condition	P_{max} (MPa)	θp_{max} (°CA)	θ_{cd} (°CA)	$\theta_{50\%}$ (°CA)	P_i (MPa)	εp_i (MPa)
X1 Experimental	2.90	377	26.87	370.42	0.794	3.75
X1 Predicted	2.88	376	27.54	370.85	0.825	
X2 Experimental	6.05	376	22.59	366.84	1.572	2.21
X2 Predicted	6.01	374	24.53	366.19	1.526	
X3 Experimental	3.74	377	23.93	366.99	1.251	1.49
X3 Predicted	3.72	376	25.03	365.74	1.270	
X4 Experimental	5.18	371	21.61	361.41	1.187	2.94
X4 Predicted	5.07	372	23.01	361.97	1.223	
X5 Experimental	4.15	374	21.02	365.49	1.042	0.478
X5 Predicted	4.17	373	23.23	365.12	1.047	
X6 Experimental	2.91	375	20.98	366.90	0.725	3.46
X6 Predicted	2.91	373	24.50	367.29	0.751	
X7 Experimental	3.38	376	28.61	370.21	0.951	1.04
X7 Predicted	3.27	376	28.58	370.70	0.961	
X8 Experimental	3.02	378	26.62	373.21	1.067	6.23
X8 Predicted	3.73	378	27.50	374.38	1.138	
X9 Experimental	3.98	376	25.38	368.10	1.085	2.43
X9 Predicted	4.06	376	26.01	369.45	1.112	

Table 6. Difference between predicted and experimental results.

http://dx.doi.org/10.5772/65753

Basically, factors influencing the simulation accuracy contain two crucial basis: first, few assumption accuracies are not steady with real condition, like chemical reaction, no heat transfer between the burned and unburned zone; second, particular errors exit in the empirical relations determining specific heat, the adiabatic flame temperature, and the laminar burning velocity. These limitations do not get notable errors in this suggested model; furthermore, they should be scrutinized well when considering precision.

Ma et al. [45] developed a fractal-based quasi-dimensional combustion model for turbocharged SI engine works on pure NG and mixtures of NG/H_2. First, they analyzed the effect of MAP, φ, and hydrogen enrichment to NG on fractal dimension and then restructured the expressions of the fractal dimensions. The original and improved two-zone combustion models have compared with the experimental data under various loads, equivalence ratios, engine speeds, and hydrogen fractions. The improved model is very near to the experimental results at the premature combustion stage. In this fractal-based model, a multiplying factor connecting the burned mass density and unburned mass density has been used as follows:

$$\frac{A_T}{A_L} = \frac{S_b}{S_L} = \left(\frac{\rho_b}{\rho_u}\right)^{0.25} \left(\frac{L_{\max}}{L_{\min}}\right)^{D_3-2}, \tag{24}$$

where ϱ_b and ϱ_u are represented by the burned and unburned mass density, and the exponent is set to 0.25, while Matthews and Chin [46] presented the comparison between three assumptions about the ratio of the flame wrinkling scales. They suggested that the reasonable assumption for the correlation between the inner and outer cutoff of the wrinkling scales was the ratio of the integral length scale to the Kolmogorov scale: $L_{max}/L_{min} = l_i/\eta$. They also stated that the following model for D_3 predicted the measured fractal dimensions of flame in combustion engines with as error of <3.6% [47].

$$D_3 = D_{3\max}\frac{u'}{u'+S_L} + 2.0\frac{S_L}{u'+S_L}, D_{3\max} = 2.35, \tag{25}$$

where u′ is denoted by turbulence intensity and S_L is the laminar burning speed. The very similar equation is used by Perini et al. [48] for forecasting of D_3 from with distinct upper limit of D_3.

$$D_3 = D_{3\max}\frac{u'}{u'+S_L} + 2.0\frac{S_L}{u'+S_L}, D_{3\max} = C_{D_3} \times 2.35, \tag{26}$$

where C_{D_3} is the calibration coefficient and is set to 1.013. Equation (35) is proved to be reasonable and acceptable for the combustion simulation of HCNG fuel [48, 49]. As per the

fractal analysis results of Ref. [50], the consequence of hydrogen portion in CNG on D_3 is added to Eq. (25) and the following equation is derived.

$$D_3 = D_{3\max}\frac{1}{1+\frac{1}{1+0.1x}\frac{S_L}{u'}} + 2.0\frac{1}{1+\frac{1}{1+0.1x}\frac{u'}{S_L}}, \tag{27}$$

where x is the hydrogen mole fraction in the HCNG. The operational condition for the tests is shown in **Table 7** for which the results of the simulation study were analyzed.

Operation condition	n (r/min)	MAP (kPa)	X	λ	θ_{ig} (BTDC
XA1	1600	70	0	1.3	28
XA2	1600	125	0	1.5	28
XA3	1600	1205	0	1.5	28
XA4	1600	70	0.15	1.3	24
XA5	1600	70	0.15	1.5	28
XA6	1600	125	0.15	1.3	20
XA7	1600	125	0.15	1.5	24
XA8	1600	70	0.3	1.3	28
XA9	1600	125	0.3	1.3	24
XA10	1600	125	0.3	1.1	20
XA11	1600	70	0.45	1.3	26
XA12	1600	70	0.45	1.5	24
XA13	1600	125	0.45	1.3	24
XA14	1600	125	0.45	1.5	22
XA15	1600	125	0.55	1.5	26
XA16	1600	125	0.55	1.3	24
XA17	1600	125	0.45	1.3	24
XB1	800	90	0.3	1.5	20
XC1	1200	110	0.3	1.5	22
XC2	1200	80	0.55	1.3	16
XD1	2000	90	0	1.4	32

Table 7. Difference between predicted and experimental result [45].

9. Demonstration projects

Because of harmful environmental consequences of the exhaust emission of the diesel/ gasoline-fuelled vehicles, several countries are committed to propose strict emission norms. Researchers are more and more focus to actualize the demands of the future's emission regulations. The HCNG engines have a promising technology for city transport system and

http://dx.doi.org/10.5772/65753

medium duty vehicles. Last few years, various governments and vehicle manufacturers are providing funds for the HCNG demonstration projects to develop the zero emission vehicles (ZEV). Various HCNG demonstration projects have been performed all around the globe. Generally, the demonstration vehicles fuelled with HCNG blends have been experimented either on the laboratory or on the on road tests [51–58].

Munshi et al. [59] developed two 40-feet-long buses with modified CWI 5.9L B Gas Plus hydrogen-enriched CNG engines for the demonstration project. They compared these two HCNG buses with two CNG buses with similar engines. On road tests and comparison of these, four buses have been performed on the same routes of SunLine Transit Agency in California, Orange County Transit Authority Cycle, and City-Suburban Heavy Vehicle Route. All buses covered the planned 24,000 miles on road test trails on regular routes (see **Figure 11**). They found that after experiments in the laboratory and on road trails, the performance of the HCNG-equipped buses is much better than that of CNG buses with significant reduction in the emissions. **Figure 12** shows HCNG demonstration projects held successfully around the world.

Figure 11. A 40-feet-long transit bus at SunLine Transit Agency with HCNG dispenser [59].

Figure 12. Various demonstration projects all around the world.

10. Conclusion

The hydrogen-enriched compressed natural gas (HCNG) has noteworthy virtues as contrasted with natural gas in terms of performance. As the hydrogen fraction increases by the effect of brake, thermal efficiency also increases. The brake specific fuel consumption is directly proportional to the cycle by cycle variations. Hence, the former is reduced; the latter also reduces, but the thermal efficiency shows increment. There are numerous optimization parameters that can be altered to adjust to the HCNG fuel. The lean operational limit expands with the improvement in hydrogen fraction. This factor maximizes the thermal efficiency and marks down the NO_x pollutants. As the increased amount of intake air introduces in the cylinder at a high excess air ratio, the combustion turns up unstable resulting more unburned hydrocarbon emission from the tailpipe. Consequently, the excess air ratio should be determined by searching the finest feasible combination of NO_x and the HC emissions. One more process to decrease an emission is to shift ignition timing near to the top dead center; in spite of the fact that this is immensely dependent on the excess air ratio. To achieve an increment in the combustion, lean limit and decrement in the HC emission, the ratio of hydrogen can be raised. The greatest obstacle to implementing this promising alternative fuel is to build an infrastructure which can support this.

The future of the HCNG vehicles is bright, and this is shown by the demonstration project, which is presented all around the world in previous years. Nevertheless, hydrogen availability at a reduced cost, its delivery, and storage infrastructure is the challenge for implementing HCNG vehicles.

Author details

Fanhua Ma* and Roopesh Kumar Mehra

*Address all correspondence to: mafh@tsinghua.edu.cn

State Key Laboratory of Automotive Safety and Energy, Tsinghua University, China

References

[1] Nagalingam B, Duebel F, Schmillen K. Performance study using natural gas, hydrogen-supplemented natural gas and hydrogen in AVL research engine. International Journal of Hydrogen Energy. 1983;8(9):715–20.

[2] Ma F, Wang Y, Liu H, Li Y, Wang J, Zhao S. Experimental study on thermal efficiency and emission characteristics of a lean burn hydrogen enriched natural gas engine. International Journal of Hydrogen Energy. 2007;32(18):5067–75.

[3] Holladay JD, Hu J, King DL, Wang Y. An overview of hydrogen production technologies. Catalysis Today. 2009;139(4):244–60.

[4] Freni S, Calogero G, Cavallaro S. Hydrogen production from methane through catalytic partial oxidation reactions. Journal of Power Sources. 2000;87(1):28–38.

[5] Hickman D, Schmidt LD. Synthesis gas formation by direct oxidation of methane over Pt monoliths. Journal of Catalysis. 1992;138(1):267–82.

[6] Balta MT, Dincer I, Hepbasli A. Potential methods for geothermal-based hydrogen production. International Journal of Hydrogen Energy. 2010;35(10):4949–61.

[7] Kanoglu M, Bolatturk A, Yilmaz C. Thermodynamic analysis of models used in hydrogen production by geothermal energy. International Journal of Hydrogen Energy. 2010;35(16):8783–91.

[8] Saxena R, Seal D, Kumar S, Goyal H. Thermo-chemical routes for hydrogen rich gas from biomass: a review. Renewable and Sustainable Energy Reviews. 2008;12(7):1909–27.

[9] Cohce M, Dincer I, Rosen M. Thermodynamic analysis of hydrogen production from biomass gasification. International Journal of Hydrogen Energy. 2010;35(10): 4970–80.

[10] Nielsen AT, Amandusson H, Bjorklund R, Dannetun H, Ejlertsson J, Ekedahl L-G, et al. Hydrogen production from organic waste. International Journal of Hydrogen Energy. 2001;26(6):547–50.

[11] Wu W, Kawamoto K, Kuramochi H. Hydrogen-rich synthesis gas production from waste wood via gasification and reforming technology for fuel cell application. Journal of Material Cycles and Waste Management. 2006;8(1):70–7.

[12] Bell SR, Gupta M. Extension of the lean operating limit for natural gas fueling of a spark ignited engine using hydrogen blending. Combustion Science and Technology. 1997;123(1–6):23–48.

[13] Tunestål P, Christensen M, Einewall P, Johansson B, Jönsson O. Hydrogen addition for improved lean burn capability of slow and fast burning natural gas combustion chambers. SAE Special Publications. 2002;2002(1725):21–32.

[14] Sharma S, Ghoshal SK. Hydrogen the future transportation fuel: from production to applications. Renewable and Sustainable Energy Reviews. 2015;43:1151–8.

[15] Koroll G, Kumar R, Bowles E. Burning velocities of hydrogen-air mixtures. Combustion and Flame. 1993;94(3):330–40.

[16] Schröder V, Holtappels K, editors. Explosion characteristics of hydrogen-air and hydrogen-oxygen mixtures at elevated pressures. In: 2nd International Conference on Hydrogen Safety; 2005.

[17] Ono R, Nifuku M, Fujiwara S, Horiguchi S, Oda T. Minimum ignition energy of hydrogen–air mixture: effects of humidity and spark duration. Journal of Electrostatics. 2007;65(2):87–93.

[18] Khan MI, Yasmin T, Shakoor A. Technical overview of compressed natural gas (CNG) as a transportation fuel. Renewable and Sustainable Energy Reviews. 2015;51:785–97.

[19] Kavathekar K, Rairikar S, Thipse S. Development of a CNG Injection Engine Compliant to Euro-IV Norms and Development Strategy for HCNG Operation. SAE Technical Paper; 2007.

[20] Coppens F, De Ruyck J, Konnov A. Effects of hydrogen enrichment on adiabatic burning velocity and NO formation in methane + air flames. Experimental Thermal and Fluid Science. 2007;31(5):437–44.

[21] Verhelst S, Woolley R, Lawes M, Sierens R. Laminar and unstable burning velocities and Markstein lengths of hydrogen–air mixtures at engine-like conditions. Proceedings of the Combustion Institute. 2005;30(1):209–16.

[22] Huang Z, Zhang Y, Zeng K, Liu B, Wang Q, Jiang D. Measurements of laminar burning velocities for natural gas–hydrogen–air mixtures. Combustion and Flame. 2006;146(1): 302–11.

[23] Ilbas M, Crayford A, Yılmaz I, Bowen P, Syred N. Laminar-burning velocities of hydrogen–air and hydrogen-methane-air mixtures: an experimental study. International Journal of Hydrogen Energy. 2006;31(12):1768–79.

[24] Halter F, Chauveau C, Djebaili-Chaumeix N, Gökalp I. Characterization of the effects of pressure and hydrogen concentration on laminar burning velocities of methane-hydrogen-air mixtures. Proceedings of the Combustion Institute. 2005;30(1):201–8.

[25] Ma F, Liu H, Wang Y, Wang J, Ding S, Zhao S. A Quasi-Dimensional Combustion Model for SI Engines Fuelled by Hydrogen Enriched Compressed Natural Gas. SAE Technical Paper; 2008.

[26] Ma F, Wang Y, Wang M, Liu H, Wang J, Ding S, et al. Development and validation of a quasi-dimensional combustion model for SI engines fuelled by HCNG with variable hydrogen fractions. International Journal of Hydrogen Energy. 2008;33(18):4863–75.

[27] Miao H, Jiao Q, Huang Z, Jiang D. Effect of initial pressure on laminar combustion characteristics of hydrogen enriched natural gas. International Journal of Hydrogen Energy. 2008;33(14):3876–85.

[28] Ma F, Wang M, Jiang L, Chen R, Deng J, Naeve N, et al. Performance and emission characteristics of a turbocharged CNG engine fueled by hydrogen-enriched compressed natural gas with high hydrogen ratio. International Journal of Hydrogen Energy. 2010;35(12):6438–47.

[29] Ma F, Wang M, Jiang L, Deng J, Chen R, Naeve N, et al. Performance and emission characteristics of a turbocharged spark-ignition hydrogen-enriched compressed natural gas engine under wide open throttle operating conditions. International Journal of Hydrogen Energy. 2010;35(22):12502–9.

[30] Ma F, Ding S, Wang Y, Wang Y, Wang J, Zhao S. Study on combustion behaviors and cycle-by-cycle variations in a turbocharged lean burn natural gas SI engine with hydrogen enrichment. International Journal of Hydrogen Energy. 2008;33(23):7245–55.

[31] Huang Z, Liu B, Zeng K, Huang Y, Jiang D, Wang X, et al. Experimental study on engine performance and emissions for an engine fueled with natural gas-hydrogen mixtures. Energy and Fuels. 2006;20(5):2131–6.

[32] Kornbluth K, Greenwood J, McCaffrey Z, Vernon D, Erickson P. Extension of the lean limit through hydrogen enrichment of a LFG-fueled spark-ignition engine and emissions reduction. International Journal of Hydrogen Energy. 2010;35(3):1412–9.

[33] Wang X, Zhang H, Yao B, Lei Y, Sun X, Wang D, et al. Experimental study on factors affecting lean combustion limit of SI engine fueled with compressed natural gas and hydrogen blends. Energy. 2012;38(1):58–65.

[34] Ma F, He Y, Deng J, Jiang L, Naeve N, Wang M, et al. Idle characteristics of a hydrogen fueled SI engine. International Journal of Hydrogen Energy. 2011;36(7):4454–60.

[35] Ma F, Li S, Zhao J, Qi Z, Deng J, Naeve N, et al. Effect of compression ratio and spark timing on the power performance and combustion characteristics of an HCNG engine. International Journal of Hydrogen Energy. 2012;37(23):18486–91.

[36] Heywood JB. Internal Combustion Engine Fundamentals. New York: McGraw-Hill; 1988.

[37] Sonntag RE, Van Wylen GJ. Introduction to Thermodynamics: Classical and Statistical. John Wiley & Sons; 1982.

[38] Blizard NC, Keck JC. Experimental and Theoretical Investigation of Turbulent Burning Model for Internal Combustion Engines. SAE Technical Paper; 1974.

[39] Lancaster DR. Effects of Engine Variables on Turbulence in a Spark-Ignition Engine. SAE Technical Paper; 1976.

[40] Tabaczynski RJ, Ferguson CR, Radhakrishnan K. A Turbulent Entrainment Model for Spark-Ignition Engine Combustion. SAE Technical Paper; 1977.

[41] Smith JR. Turbulent Flame Structure in a Homogeneous-Charge Engine. SAE Technical Paper; 1982.

[42] Daneshyar H, Hill P. The structure of small-scale turbulence and its effect on combustion in spark ignition engines. Progress in Energy and Combustion Science. 1987;13(1): 47–73.

[43] Tabaczynski RJ, Trinker FH, Shannon BA. Further refinement and validation of a turbulent flame propagation model for spark-ignition engines. Combustion and Flame. 1980;39(2):111–21.

[44] Wahiduzzaman S, Moral T, Sheard S. Comparison of Measured and Predicted Combustion Characteristics of a Four-Valve SI Engine. SAE Technical Paper; 1993.

[45] Ma F, Li S, Zhao J, Qi Z, Deng J, Naeve N, et al. A fractal-based quasi-dimensional combustion model for SI engines fuelled by hydrogen enriched compressed natural gas. International Journal of Hydrogen Energy. 2012;37(12):9892–901.

[46] Matthews RD, Chin Y-W. A Fractal-Based SI Engine Model: Comparisons of Predictions with Experimental Data. SAE Technical Paper; 1991.

[47] CHIN Y-W, Matthews RD, Nichols SP, Kiehne TM. Use of fractal geometry to model turbulent combustion in SI engines. Combustion Science and Technology. 1992;86(1–6):1–30.

[48] Perini F, Paltrinieri F, Mattarelli E. A quasi-dimensional combustion model for performance and emissions of SI engines running on hydrogen-methane blends. International Journal of Hydrogen Energy. 2010;35(10):4687–701.

[49] Verhelst S, Sierens R. A quasi-dimensional model for the power cycle of a hydrogen-fuelled ICE. International Journal of Hydrogen Energy. 2007;32(15):3545–54.

[50] Cohé C, Halter F, Chauveau C, Gökalp I, Gülder ÖL. Fractal characterisation of high-pressure and hydrogen-enriched CH 4–air turbulent premixed flames. Proceedings of the Combustion Institute. 2007;31(1):1345–52.

[51] Burke A, McCaffrey Z, Miller M, Collier K, Mulligan N. Hydrogen Bus Technology Validation Program. Institute of Transportation Studies; 2005.

[52] Dalhuijsen W, Bosma H, Merts M, Buning L. Internal Combustion Engine Vehicle: Emissions and Performance Using Blends of Natural Gas and Hydrogen. SAE Technical Paper; 2007.

[53] Munshi S, Gourley D, editors. HCNG engine powered transit buses operating on waste hydrogen. In: The NHA Annual Hydrogen Conference 2008; 2008.

[54] Eichlseder H, Klell M, Schaffer K, Leitner D, Sartory M. Potential of Synergies in a Vehicle for Variable Mixtures of CNG and Hydrogen. SAE Paper; 2009.

[55] Khatri D, Singh V, Pal N, Maheshwari M, Singh S, Chug S, et al. HCNG Evaluation Using a Sequential Gas Injection System for a Passenger Car. SAE Technical Paper; 2009.

[56] Unich A, Morrone B, Mariani A, Prati M. The Impact of Natural Gas-Hydrogen Blends on Internal Combustion Engines Performance and Emissions. SAE Technical Paper; 2009.

[57] Genovese A, Contrisciani N, Ortenzi F, Cazzola V. On road experimental tests of hydrogen/natural gas blends on transit buses. International Journal of Hydrogen Energy. 2011;36(2):1775–83.

[58] GRHYD Demonstration Project. www.engie.com. 2013.

[59] Munshi S, Nedelcu C, Harris J, Edwards T, Williams J, Lynch F, et al. Hydrogen Blended Natural Gas Operation of a Heavy Duty Turbocharged Lean Burn Spark Ignition Engine. SAE Technical Paper; 2004.

IntechOpen